J Mater Sci (2009) 44:2590–2598
DOI 10.1007/s10853-009-3339-5

Elasto-plastic properties of gold thin films deposited onto polymeric substrates

F. Avilés · L. Llanes · A. I. Oliva

Received: 15 October 2008 / Accepted: 10 February 2009 / Published online: 6 March 2009

Abstract This work examines mechanical properties of 50–300 nm gold thin films deposited onto micrometer-thick flexible polymer substrates by means of tensile testing of the film–substrate system and modeling. The film properties are extracted from mechanical testing of the film–substrate system and modeling of the bimaterial. Unlike materials in bulk geometry, the film elastic modulus and yield strength present an important dependence with film thickness, with modulus and yield strength of about 520 and 30 GPa, respectively, for the thinner films and decreasing toward the bulk value as the film thickness increases. The relation between grain size, film thickness, and yield strength is examined. Finite element analysis provides further insight into the stress distribution in the film–substrate system.

Introduction

Given the fast growth and new challenges of nano-technology, metallic and non-metallic thin films are nowadays receiving renewed attention in the scientific and technological community all over the world. Metallic films are typically employed as coatings and interconnections in microelectronics, solar cells, optical waveguides, photolithographic masks, solid state devices, bioengineering, and electronic textiles (E-textiles), among many others [1–5]. E-textiles, for example, are textiles that possess tiny flexible electronic sensors and devices embedded into a fabric to build human–device communication interfaces. Those micro-circuits can be used, for example, to monitor the steps of a jogger [6]. The new trends of nano-, micro-, and macroelectronics demand portability and flexibility, and flexible polymeric materials are ideal candidates for such a task. Although mechanical properties of metallic films have been studied to some extend, they are conventionally deposited over rigid and brittle substrates (e.g., silicon). Experimental work as well as molecular dynamics simulations point out that the elasto-plastic behavior of thin metallic films with grain sizes in the nanometric range can differ significantly to the mechanical behavior of coarse grain materials [7–9]. As stated by Meyers et al. [8], for "large" grain materials ($d > 1$ μm) the mechanisms governing plastic deformation are mostly work hardening and unit dislocation grain. For very small grain sizes ($d < 10$ nm), intragranular dislocation activity occurs and grain boundary shear may be the dominant mechanism of deformation. The intermediate grain size ($10\text{ nm} < d < 1$ μm), may possess contributions from both regimes, and thus is the less understood. It has also been observed that the substrate may play an important role on the mechanical properties of the film, suggesting that the film mechanical properties depend on the substrate employed and thus further motivating the study of thin metallic films over flexible polymer substrates [10, 11]. The most common methods employed for determination of film mechanical properties are maybe those based on

L. Llanes—MS student at ITM, Merida, Mexico.

F. Avilés (✉) · L. Llanes
Unidad de Materiales, Centro de Investigación Científica de Yucatán, A.C., Calle 43 # 103, Col. Chuburná de Hidalgo, 97200 Mérida, Yucatán, México
e-mail: faviles@cicy.mx

A. I. Oliva
Departamento de Física Aplicada, Centro de Investigación y de Estudios Avanzados del IPN, Unidad Mérida, A.P. 73 Cordemex, 97310 Mérida, Yucatán, México

thermal bending, X-ray diffraction, and nanoindentation [12–15]. Some research efforts have also been conducted employing direct mechanical testing of the film–substrate (bimaterial) system or free-standing films [16–19]. Yu and Spaepen [19] investigated the behavior of yield strength in 0.25–2.85 μm Cu films over thin Kapton deposited by electron beam evaporation. They found a strong dependence of the yield strength with film thickness, which do not follow the well-known Hall-Petch relation [20, 21]. The yield strength of the films examined in their work showed a weak dependence with the grain size and the increase in yield with decreased film thickness was attributed to a "thickness effect". The film Young's modulus in Yu and Spaepen's work, however, resulted fairly independent of the film thickness, at least in the thickness range examined. Macionzyk and Bruckner [22] observed a Hall-Petch-type relation between the yield strength and grain size by tensile testing 0.2–2 μm Al–Cu films sputtered over a thin polyimide film, while the film elastic modulus was close to the bulk value. Some other works report that the elastic modulus of metallic nanostructures increase with decreased thickness [23, 24]. Thus, it is clear that the mechanical properties of thin films are overall dependent on the film thickness and microstructure. The functional form of this relation depends on several factors such as deposition technique, amount of residual stresses, film texture, and grain size, and thus they are still a matter of controversy.

In this study, 50–300 nm gold thin films were deposited over two flexible polymer substrates and their mechanical properties were investigated through tensile testing of the film–substrate bimaterial and modeling. The size-dependence of the mechanical properties and their relation to grain size and film thickness are investigated. Finite element analysis is also conducted to shed some light on the stress distribution in the film–substrate system.

Experimental

Polymer substrate manufacturing

A commercial thermoplastic, Polysulfone (PSF) [25], and a home-synthesized isophthalic polyester based on the reaction of 4,4′-(1-hydroxyphenylidene) phenol and isophthaloyl dichloride (hereon referred to as "BAP") [26] were used as raw materials for substrate production. Both materials present excellent thermal properties, which permits the substrate to withstand the temperatures achieved during film deposition by PVD (thermal deposition). Films were prepared by solution casting from solutions containing 0.9 g of the polymer dissolved in 14 mL of dichloromethane. After dissolving the polymer, the solution was poured into prefabricated aluminum rings (molds) located on top of a smooth glass plate and maintained under dichloromethane atmosphere. After evaporating the chloroform, the polymer films (about 80 μm thick) were taken out of the mold and dried in an oven at 100 °C for 24 h, to eliminate possible remaining solvent. Polymer substrates for film deposition were then cut to rectangular shapes of nominal dimensions 30 mm × 5 mm × 80 μm.

Film deposition

High purity (99.999%) gold splatters from CERAC^{TM} were used for film deposition. Prior to deposition, the substrates were cleaned in steps with soap, isopropyl alcohol and rinsed with distilled water between each step. Gold films with thickness of 50, 100, 200, and 300 nm were deposited onto PSF substrates by thermal evaporation inside a vacuum chamber at 3×10^{-5} Torr. The deposition rate was 0.5 nm/s, controlled with a Maxtek TM-400 thickness monitor and a quartz crystal. The source-to-substrate distance within the vacuum chamber was 25 cm. To investigate a possible substrate effect, a group of films with thicknesses of 100 nm were deposited over BAP substrates. All films of the same thickness were deposited at the same time using a four replicate testing program.

Tensile testing

Tensile testing of Au/PSF (film thicknesses, 50–300 nm) and Au/BAP (film thickness, 100 nm) specimens was conducted to investigate the mechanical properties of the Au films. Tests of the as-fabricated PSF and BAP substrates (6 replicates) were also conducted as a baseline. Tensile testing was conducted in a small testing machine with a load cell of 200 N and a cross-head speed of 0.05 mm/min. The strain was calculated from the cross-head displacement of the testing machine. The substrate and bimaterial specimens were nominally 30 mm long and 5 mm wide with a span length of 20 mm. The nominal substrate thickness was 80 μm for both types of substrates employed.

Determination of film properties

The film mechanical properties were extracted from the tensile response of the film/substrate system, considered as a bimaterial. A simple "strength of materials" formulation based on sum of forces and strain compatibility was used to extract the film stress from the stress applied to the bimaterial and generate stress–strain curves for the film. Iterative finite element analysis of the bimaterial, allowed further verification of the film elastic modulus as well as

determination of the stress distribution in the film–substrate system. Details of both analyses are discussed below.

Strength of materials formulation

Consider a film(f)–substrate(s) bimaterial as that sketched in Fig. 1. The bimaterial has a length L, total thickness t ($= t_f + t_s$), and width w ($= w_f = w_s$). When a total force P is applied to the film–substrate bimaterial the force is carried by the film and substrate such as,

$$P = P_f + P_s \tag{1}$$

The total strain applied (ε), on the other hand, is the same for both material, i.e.,

$$\varepsilon = \varepsilon_f = \varepsilon_s \tag{2}$$

Using the one-dimensional Hooke's law for stress–strain for each material component, along with Eqs. 1 and 2 we obtain,

$$E_f = \frac{1}{A_f}[A_{Bim}E_{Bim} - A_sE_s] = \left(1 + \frac{t_s}{t_f}\right)E_{Bim} - \left(\frac{t_s}{t_f}\right)E_s \tag{3}$$

where $A = wt$ is the cross-sectional area and sub-index "Bim" corresponds to the film–substrate bimaterial ($A_{Bim} = w(t_s + t_f)$).

Using Eq. 1 and the common definition of stress ($\sigma = P/A$), the film stress can be obtained subtracting the substrate contribution from the total (applied) force,

$$\sigma_f = \frac{1}{A_f}[P - P_s] = \left(1 + \frac{t_s}{t_f}\right)\sigma_{Bim} - \left(\frac{t_s}{t_f}\right)\sigma_s \tag{4}$$

where σ_f and σ_s are the film and substrate stresses, respectively, and σ_{Bim} is the total stress applied to the bimaterial ($\sigma_{Bim} = P/w(t_s + t_f)$).

Notice the importance of the t_s/t_f ratio in the relative contribution of the film and substrate to the mechanical response of the bimaterial. Equations 3 and 4 can also be derived in terms of forces.

Usually, the substrate thickness is much greater than the film thickness. For cases where $t_s \gg t_f$, Eqs. 3 and 4 simplify to,

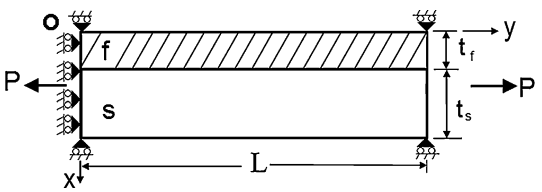

Fig. 1 Schematic representation of the film/substrate bimaterial system examined

$$E_f = \left(\frac{t_s}{t_f}\right)(E_{Bim} - E_s) \tag{5a}$$

$$\sigma_f = \left(\frac{t_s}{t_f}\right)(\sigma_{Bim} - \sigma_s) \tag{5b}$$

Thus, if the specimen geometry is known and the bimaterial and substrate are tested recording stress–strain curves, Eqs. 3 and 4 (or Eqs. 5a and 5b, if $t_s \gg t_f$) allow determination of the film elastic modulus and construction of the film stress–strain curve. In this sense, the film mechanical properties are obtained by difference between the substrate and bimaterial curves. It is worth to mention that this simple model predicts the film mechanical response based on the bimaterial one; thus, any localized effect which is not transferred to the stress–strain bimaterial response would not be detected by this macroscopic model.

Finite Element Analysis

Two-dimensional linear elastic finite element analysis (FEA) was conducted to obtain the elastic modulus and stress distribution of 50–300 nm gold (Au) films deposited onto 80 μm PSF substrates. Four-node linear interpolation elements configured in plane stress were used for the film and substrate. Each node of the element possess two translational degrees of freedom, viz. displacements in the x and y directions. The actual specimens have a span length of 20 mm, a nominal width (w) of 5 mm, and a nominal substrate thickness (t_s) of 80 μm. Since the model is two-dimensional, the specimen width is used solely to scale the predicted (unit width) displacement. Taking advantage of the specimen symmetry, only 1/40 of the actual span length (0.50 mm) was modeled. This simplification greatly reduces the number of elements without changing the results respect to a full model. The modeled specimen length (0.50 mm) was uniformly divided in the longitudinal (y) direction into 500 ($t_f = 300$ and 200 nm) or 1000 elements ($t_f = 100$ and 50 nm), depending on the film thickness. The different number of divisions in the longitudinal direction was necessary to keep the elements aspect ratio below 20. Two elements were used for the film in the through-thickness (x) direction and a graded mesh was used for the through-thickness substrate elements. For the substrate, the thinnest elements share nodes with the film ones and the thicker elements are located at the free surface. The smallest substrate elements were of identical width to the film ones ($t_f/2$), while the larger ones were about 3.5 μm wide. Thus, a typical model ($t_f = 100$ nm) employed about 32,000 elements. The actual FEA mesh is too dense to visualize in a full picture of the model, and thus it is not shown. The bottom of the film/substrate system was enforced to zero displacements in the y direction, simulating the clamping

action of a tensile test rig. The corner nodes at the top (load introduction) and bottom (clamped) edges of the specimen were constrained to zero displacements in the transverse (x) direction. To simulate uniform load introduction, all nodes located at the top edge were constrained to have equal displacement in the y-direction. A unit load ($P = 1$ N/m) was applied to the top edge of the model. The elastic modulus and Poisson's ratio of the PSF substrate used in the FEA were 735 MPa (measured) and 0.37 [25]. The Poisson's ratio of the film was fixed at 0.38, according to previous publications for (111) gold [27]. Since the film modulus is unknown, an iterative process was established for its determination via FEA. The procedure followed is detailed in Ref. [28] and thus it will only be briefly outlined here. In this method, a value of E_f is first assumed, FEA is conducted and the elastic modulus of the film/substrate bimaterial (E_{Bim}) is calculated from the predicted displacement response of the bimaterial. The assumed value of the film modulus is then changed and the process repeated, generating an E_f versus E_{Bim} curve. The value of E_f that produces a value of E_{Bim} equal to that measured during the film/substrate bimaterial tensile test corresponds to the film elastic modulus predicted by FEA.

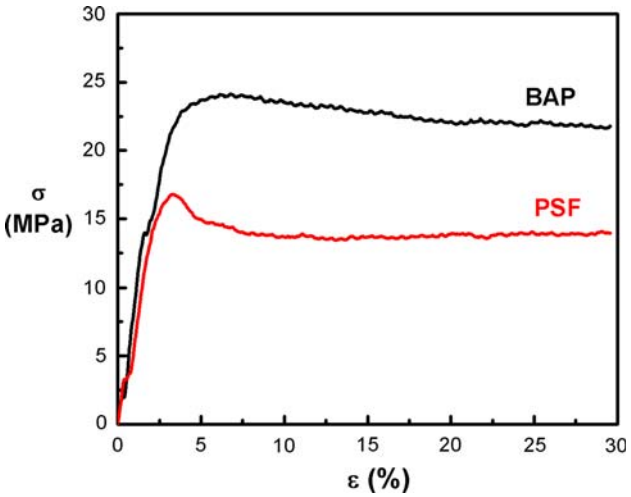

Fig. 2 Tensile stress–strain curves for PSF and BAP substrates

Table 1 Mechanical properties of the examined substrates

Material	E (MPa)	σ_{max} (MPa)	ε_{ult} (%)
PSF	735 ± 36.1	16.9 ± 2.76	27.6 ± 4.9
BAP	864 ± 30.4	24.5 ± 2.26	28.8 ± 2.5

Results and discussion

Elasto-plastic properties of films

The mechanical response of the substrates was characterized first. Figure 2 shows representative stress–strain curves of the PSF and BAP substrates. The average and standard deviation values of strength, ultimate strain, and elastic modulus are summarized in Table 1. The elastic modulus was obtained from the initial slope (0.3–1.5%) of the curves. Lower deformation levels (<0.3%) were not used for modulus calculation since the difficulty to mount such thin samples perfectly tautly in the test rig prohibited extraction of meaningful data in that region. Both materials show a linear elastic region at low attained strain followed by a plastic region at large deformations. The BAP substrate present markedly higher strength and slightly higher modulus than the PSF one. The lower strength and modulus of PSF with respect to BAP, however, may be beneficial to extract the film properties from the bimaterial response, since stiff and strong substrates may hinder the extraction of mechanical properties of the film employing the method proposed herein. Selected curves of the tensile response of the film/substrate bimaterials examined are shown in Fig. 3. The mechanical response of Au/PSF bimaterials of different film thickness is shown in Fig. 3a, while the response of the 100 nm Au film over a BAP substrate is shown in Fig. 3b. The substrate curve is plotted as a reference in Fig. 3. Failure occurred by film cracking and loss of load bearing capacity, although the polymeric substrate did not always fracture into two parts. A marked increase in strength with respect to the substrate was observed for all bimaterials, regardless of the substrate employed and film thickness. As shown in Fig. 3, the ultimate strain of the bimaterial (~4.5% for Au/PSF), is substantially reduced with respect to that of the substrate (>10%), since the film ultimate strain is low and hampers further deformation of the bimaterial. It is known that free-standing films deform only a few percentage, typically below 2% [17, 29]. The increased film ductility observed in the film/substrate system is provided by the flexible substrate, as discussed in previous publications [10, 11]. This is a clear indication that the film mechanical properties are substrate dependent. Furthermore, the Au/PSF (Fig. 3a) and Au/BAP (Fig. 3b) curves for $t_f = 100$ nm are somewhat different, with the BAP system providing improved mechanical properties.

Stress–strain curves of Au films of different thicknesses were extracted using the analytical method introduced above, Eq. 5b. Figure 4 shows representative Au film curves for each film thickness examined herein, extracted from the curves of the Au/PSF bimaterials ($t_f = 50$–300 nm, solid lines) and from the Au/BAP ones ($t_f = 100$ nm, marked with empty circles). The curves selected are the closer ones to the average values of all replicates tested. From the curves extracted from the

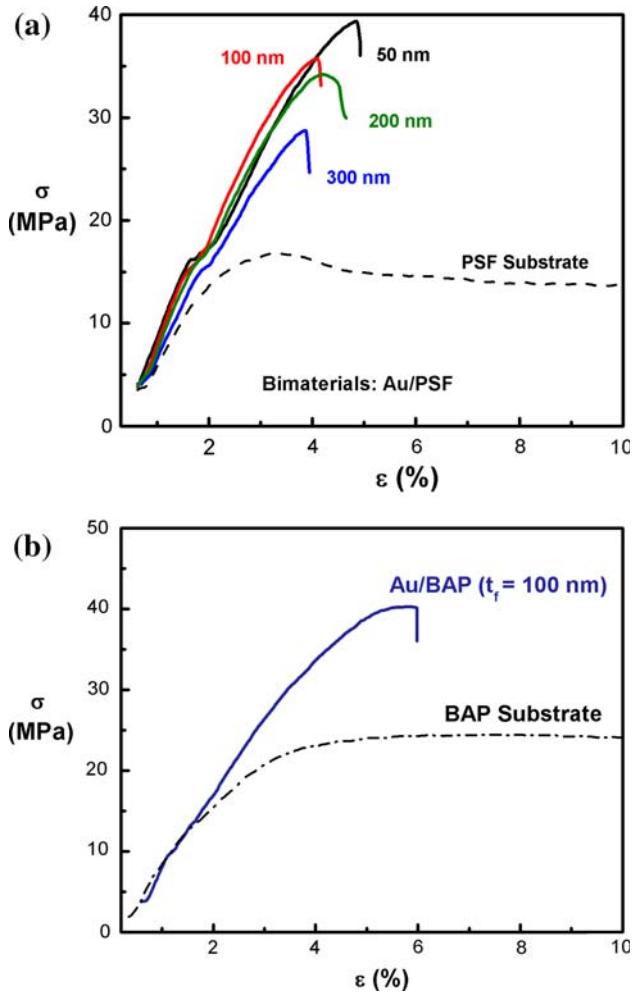

Fig. 3 Tensile stress–strain curves for (**a**) Au/PSF bimaterials, (**b**) Au/BAP bimaterial ($t_f = 100$ nm)

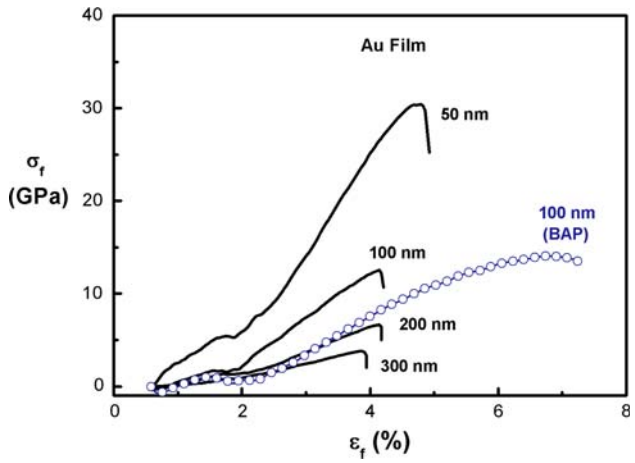

Fig. 4 Stress–strain curves for Au films extracted from the difference between Au/PSF and PSF (substrate) curves, Eq. 5b

Au/PSF system, it is clear that the film thickness has a marked influence on the strength and elastic modulus of the film, with thinner films presenting superior mechanical performance. Interestingly, the mechanical behavior of films with $t_f = 100$ nm extracted from the Au/PSF and Au/BAP systems show important differences, with increased strength and ultimate deformation (and thus toughness) for the films deposited over the BAP substrates. The plastic zone of the films deposited over the PSF substrates is very much reduced, while a larger plastic zone is observed for identical film thickness deposited over BAP. The increased toughness of the Au film deposited over the BAP substrate further suggests that the film mechanical properties are substrate dependent.

Since the plastic zone of the Au films deposited over PSF substrates is very limited, the offset method [30] was used to determine its yield strength. In this method, a strain offset is fixed (typically 0.2%) and a straight line parallel to the initial slope of the σ–ε curve is drawn starting from the offset point. The yield point is determined as the point where the straight line intersects the actual σ–ε curve. For the case of the Au films extracted from the Au/PSF system (solid curves in Fig. 4), the value of the yield strength and strain determined in this manner are very close to the maximum stress (strength) and ultimate strain, given the reduced extension of the plastic zone. For the 100 nm Au films extracted from the Au/BAP system (curve with empty circles in Fig. 4), on the other hand, the film yield strength occurs at about 85% of the maximum stress experienced by the film.

Film elastic modulus (Eq. 5a) and yield strength (0.2% offset) versus film thickness are plotted in Fig. 5. Both curves were obtained from Au/PSF. The film elastic modulus (Fig. 5a) is about 520 GPa for 50 nm thick films and decreases as the film thickness increases, approaching typical values of gold in bulk geometry (77 GPa [31]) for film thickness of 300 nm. The dependence of film Young's modulus with film thickness is a nonlinear relation which may be influenced by the film microstructure, confinement effects, and deposition method. The yield strength also shows a dependency with the film thickness, presenting significantly larger values of yield strength for the thinner (50 nm) films. The mean yield strength predicted for the 50 nm thick films is 30.2 GPa, while that for the 300 nm thick film is 3.85 GPa. These values are substantially higher than the bulk value of 205 MPa reported in the literature [31–34]. The average elastic modulus, yield strength, and maximum stress of the 100 nm thick Au films deposited over the BAP substrate were 271, 13.7, and 15.4 GPa, respectively. The difference of these values with the corresponding values for Au films of the same thickness but deposited over PSF substrates (367, 9.47, and 9.55 GPa, respectively) further highlights the substrate

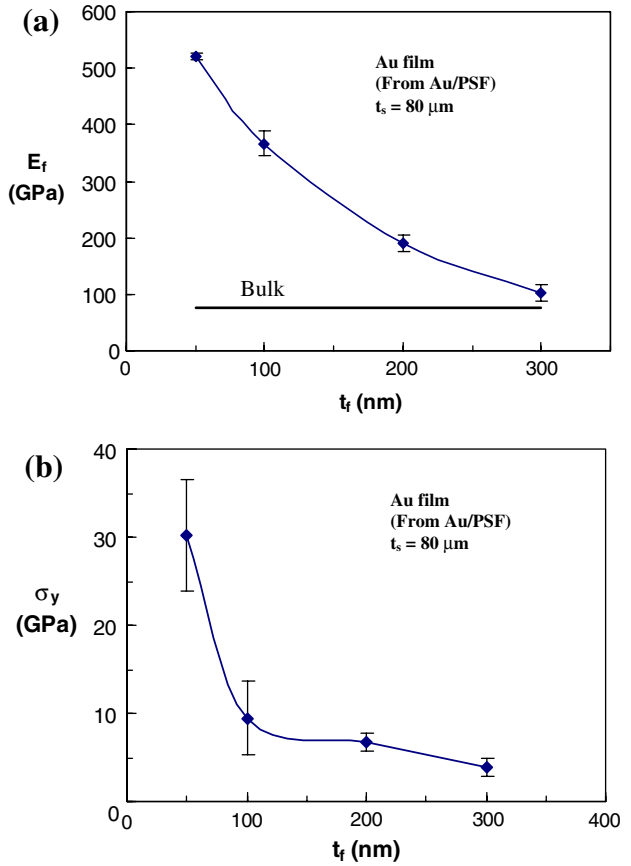

Fig. 5 Film elastic modulus (**a**) and 0.2% offset yield strength (**b**) versus film thickness

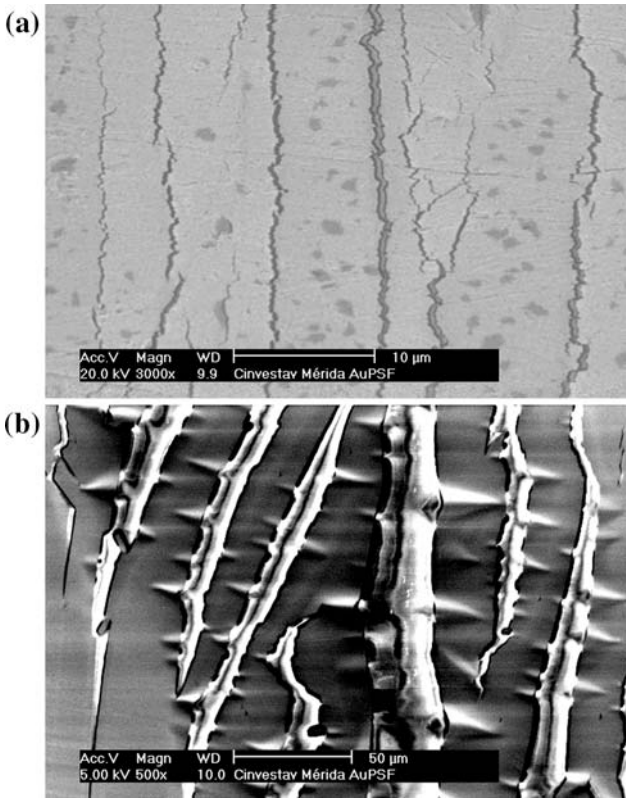

Fig. 6 Fracture surfaces of Au films over PSF substrates. (**a**) t_f = 50 nm, (**b**) t_f = 200 nm

effect on the film mechanical properties. Some previous results for nanostructured gold [33, 35–37] also report high values of elastic modulus and yield strength.

SEM images of the films surface after testing were obtained to investigate their fracture characteristics. Figure 6 shows images of the film fracture surface for film thickness of 50 (Fig. 6a) and 200 nm (Fig. 6b) deposited over PSF. Irrespective of film thickness and substrate, the fracture lines were observed forming angles ranging between 60° and 90° with the direction of the applied load (horizontal direction in Fig. 6), typical from cracks induced by tension stresses. For the thinner films (Fig. 6a, scale bar 10 μm), the observed cracks are very narrow and shallow as compared to those cracks observed for 200 and 300 nm thick films (Fig. 6b, scale bar 50 μm). As observed in Fig. 6b, the thicker films show a large extend of film delamination, evidenced by the bright branching markings adjacent to the crack lines. The cause of these delaminations may be residual stresses build up during film deposition. It is likely that a large amount of through-thickness residual stresses accumulate during film deposition, which tend to release during tensile loading of the film. The residual stresses build up during deposition should be more severe for thicker films, promoting delamination and earlier failure for thicker films. Obviously, the amount of residual stresses depends on the deposition method.

Grain size dependence

In order to investigate a possible correlation between the film microstructure and its yield strength, AFM images of the film surface of as-grown samples were taken. Larger grain sizes were observed for thicker films. Figure 7 shows representative images (1 μm × 1 μm) of the surface topography for films of 50 (Fig. 7a) and 300 nm thickness (Fig. 7b), where larger grains are observed for the thickest film. The dependence of grain size with film thickness is shown in Fig. 8a. The average grain size increases from 83 to 133 nm when the film thickness is increased from 50 to 300 nm. Although Fig. 8a evidences a dependence of the grain size with film thickness, the observed dependence seems to be relatively weak to justify the steep increase in yield strength with decreased film thickness, see Fig. 5b. For bulk materials, the relation between grain size (d) and yield strength (σ_y) typically follows the well-known Hall-Petch relation [20, 21],

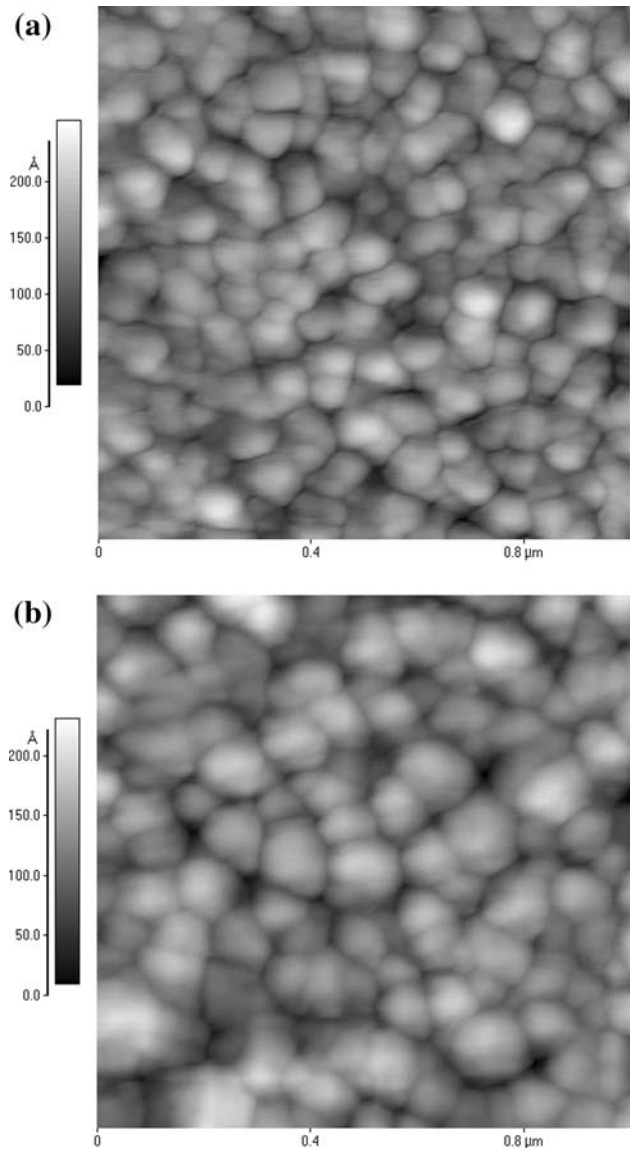

Fig. 7 AFM micrographies of as-deposited Au films over a PSF substrate. Image size is 1 μm × 1 μm. (**a**) $t_f = 50$ nm, (**b**) $t_f = 300$ nm

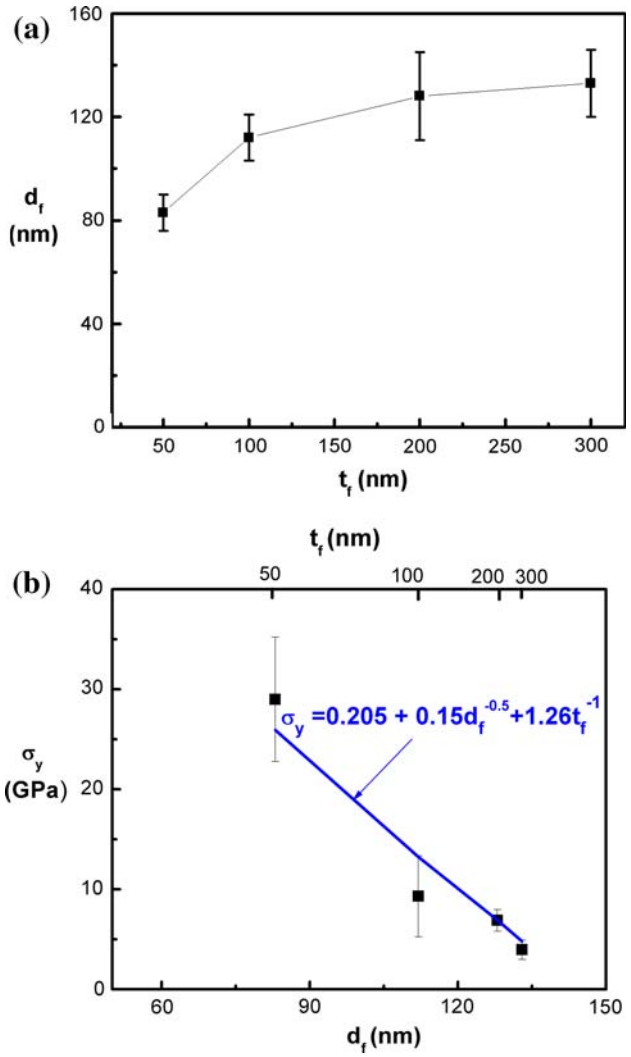

Fig. 8 Relation between film thickness, grain size, and yield strength for Au films over PSF substrates. (**a**) Film thickness vs. grain size, (**b**) grain size vs. yield strength

$$\sigma_y = \sigma_o + k_1 d^{-n} \tag{6}$$

where σ_o is the stress required to activate the gliding process, k_1 is the Hall-Petch coefficient of the material, and $n = 0.5$ is the Hall-Petch exponent, as originally proposed by these two authors. The first term in Eq. 6 represents the bulk yield strength for large grained polycrystals, while the second one represents the contribution from the grain boundaries. It has been proposed that for thin films with very fine grains ($d_f \ll t_f$) the Hall-Petch exponent (n) may differ to 0.5 [19]. It is also argued that for thin films, the film thickness (film–substrate interface) may cause confinement effects which affect the yield strength of the film. Thus, it has been proposed that the grain size and film-thickness contributions to the film yield strength may be expressed as a generalization of the Hall-Petch relation, i.e., [19],

$$\sigma_y = \sigma_o + k_1 d_f^{-n} + k_2 t_f^{-m} \tag{7}$$

where the exponent "n" may divert from 0.5 and the parameters "m" and k_2 quantify the thickness contribution. In reality, unless the grain size is independent of film thickness, both effects are intrinsically related and may be difficult to isolate. The dependence of the yield strength with grain size for the Au films over PSF substrates examined herein is shown in Fig. 8b. For our particular case, the yield strength of the Au films cannot be fitted to a Hall-Petch-type relation, Eq. 6, irrespective of the coefficient n used ($0 < n \leq 1$). The values of σ_y produced using Eq. 6 are overly low, indicating that grain size is not the microstructural parameter governing yield strength in this case, and

additional effects should account for the dependence of yield strength with film thickness. A better fit to the experimentally determined values was achieved by fixing $\sigma_o =$ 205 MPa and $n = 0.5$, and varying the parameters k_1, k_2, and m in Eq. 7. The best fit obtained (solid line in Fig. 8b) corresponds to k_1 = 150 MPa $\mu m^{0.5}$ (0.15×10^6 $Nm^{-3/2}$), k_2 = 1.26 GPa μm (1.26×10^3 Nm^{-1}), and m = 1.

Reasonable variations in the values chosen for σ_o and n did not produce further improvements in the fit. The values found for these parameters are in the range of those found for other material systems, where the film thickness exponent m was found to be 1 [19, 38, 39]. This indicates that, for our case, the confinement effect caused by the free surface of the thin film and film/substrate interface influence the film yield strength much stronger than the grain size. As observed in Figs. 5 and 8 this effect is particularly important for the thinner (50 nm) films. As mentioned previously, residual stresses in the film arising from film deposition may considerably affect the film yield strength. The increase in yield strength for thin films has also been explained using crystal plasticity models by variations in the grain orientations through the film thickness, as well as surface hardness due to oxidation [40].

Finite element investigation

The film elastic modulus was determined by FEA using the iterative process described previously. FEA predictions of the film modulus for each film thickness of the Au/PSF system examined herein are presented in Table 2, along with the predictions of the strength of materials formulation, Eq. 5a. Remarkable agreement between FEA predictions and those from the strength of materials formulation are observed. It is important to highlight that both formulations rely on determination of the substrate and bimaterial modulus from separate tensile testing. The film elastic modulus increases as the film thickness decreases, which may be caused by thickness confinement effects that create strain gradients within the thin film which modify the elastic response of the material.

In order to investigate the stress distribution in the film and substrate, the film elastic modulus determined from FEA (Table 2) was fed into the model along with the substrate modulus (E_s = 735 MPa). A unit stress σ_o was applied by means of a unit tensile load (P = 1 N/m) applied to the bimaterial and the stress distribution was extracted by mapping the nodal stresses into a predefined path, located at a cross section at the mid-length ($y = L/2$). Figure 9 presents the longitudinal (σ_y) and transverse shear (τ_{xy}) stress distribution normalized by the applied (unit) stress σ_o, for the four film thicknesses examined in this study. As shown in Fig. 1, the x-coordinate here represents the through-thickness (transverse) direction, with $x = 0$ corresponding to the free surface of the film, and $x = 80$ μm + t_f corresponding to the free surface of the substrate. Since the coordinate x is the through-thickness direction, τ_{xy} represents an interlaminar stress. The longitudinal stress distribution, Fig. 9a, evidences that a large amount of the applied stress is carried by the thin film, which decays rapidly to a plateau region of constant stress within the substrate. Thus a large amount of the applied stress is carried by a thin region of high modulus (film) while the remaining stress is more evenly distributed

Table 2 Au film elastic modulus predicted using FEA and Eq. 5a

t_f (nm)	E_f (GPa)	
	FEA	Eq. 5a
50	519	522
100	354	367
200	189	191
300	102	102

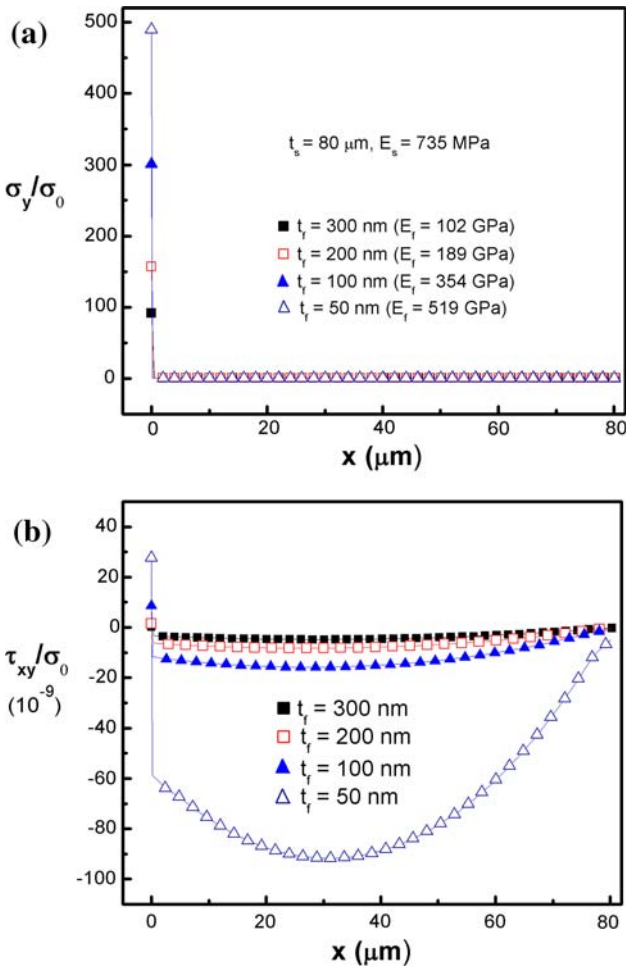

Fig. 9 Stress distribution in Au/PSF bimaterials as a function of the thickness coordinate (x). (**a**) Longitudinal stress (σ_y), (**b**) transverse shear stress (τ_{xy})

within the thicker and more compliant substrate. The peak stress reached in the film increases as the film thickness decreases, as a consequence of the higher elastic modulus employed for the thinner films. For the transverse shear stress, Fig. 9b, the symmetric parabolic distribution expected for a homogeneous material is disrupted by the presence of the thin and stiff film, causing a steep jump in stress followed by a smoother parabolic distribution within the substrate. As for the longitudinal stress, the peak stress is larger for thinner films due to their higher modulus. Although transverse shear stresses certainly promote film delamination, the low magnitude of τ_{xy} attained with respect to the applied stress ($\tau_{xy}/\sigma_0 \sim 10^{-9}$) suggests that this stress by itself is not the one triggering film delamination. Therefore, additional effects such as residual stresses build up during film deposition should be the ones causing film delamination of the thicker films, Fig. 6b, as pointed out previously.

Conclusions

Mechanical properties of 50–300 nm thick Au films over two different flexible polymer substrates (PSF and BAP) have been examined experimentally and numerically. Contrary to large grained bulk materials, the film elastic modulus and yield strength were found to depend on the film thickness, with thinner films presenting stiffer and stronger behavior. The stress distribution predicted by FEA confirm the larger load bearing capacity of thinner films. The film elasto-plastic properties were somewhat different depending on the polymer substrate employed, suggesting that the substrate mechanical properties influence the film ones. Thus, the mechanical properties of thin films are believed to be substrate dependent, at least to certain extend. The relation between film yield strength and grain size did not follow the Hall-Petch relation, and additional effects such as film thickness seem to play a more important role on the film yield strength. Several reasons such as deposition method, substrate type, processing parameters, thermal history, intrinsic (residual) stresses, thickness confinement, grain size, and maybe other microstructrual parameters can strongly affect the elasto-plastic behavior of thin metallic films. Determination of each individual contribution demands further investigation.

Acknowledgements This work was partially supported by CONACYT (Mexico) through project numbers F1-54173 and 79609. The authors deeply appreciate technical advice and know-how on polymer membrane (substrate) manufacturing by solution casting from Dr Manuel Aguilar and María Bastarrachea at CICY. The authors are also grateful to Alejandro May (CICY), Emilio Corona, and Oscar Ceh (CINVESTAV-Merida) for their technical support.

References

1. Maluf N (2000) An introduction to microelectromechanical systems engineering. Artech House, Boston
2. Liu F, Rugheimer P, Mateeva E, Savage DE, Lagally MG (2002) Nature 416:498
3. Lumelsky VJ, Shur MS, Wagner S (2001) IEEE Sens 1:41
4. Bonderover E, Wagner S (2004) IEEE Electron Device Lett 25:295
5. Mendelsohn J, Yang SY, Hiller J, Hochbaum A, Rubner MF (2003) Biomacromolecules 4:96
6. Diamond D (2008) Introducing sensing capabilities into textiles. In: 3rd International Conference for Industry, Healthcare and Fashion. The Royal Society, London
7. Rajagopalan J, Han JH, Saif MTA (2007) Science 315:1831
8. Meyers MA, Mishra A, Benson DJ (2006) Prog Mater Sci 51:427
9. Greer JR, Oliver WC, Nix WD (2005) Acta Mater 53:1821
10. Xiang Y, Li T, Suo Z, Vlassaka JJ (2005) Appl Phys Lett 87:161910
11. Li T, Suo Z (2006) Int J Solids Struct 43:2351
12. Retajczyk TF, Sinha AK (1980) Appl Phys Lett 36:161
13. Goudeau P, Renault PO, Villain P, Coupeau C, Pelosin V, Boubeker B, Badawi K F, Thiaudiere D, Gailhanou M (2001) Thin Solid Films 398–399:496
14. Bucaille JL, Stauss S, Schwaller P, Michler J (2004) Thin Solid Films 447–448:239
15. Oommen B, Van Vliet KJ (2006) Thin Solid Films 513:235
16. Sharpe WN Jr, Yuan B, Edwards RL (1997) J Microlectromech Syst 6:193
17. Huang H, Spaepen F (2000) Acta Mater 48:3261
18. Faurie D, Renault PO, Le Bourhis E, Goudeau Ph (2006) Acta Mater 54:4503
19. Yu DYW, Spaepen F (2003) J Appl Phys 95:2991
20. Hall EO (1951) Proc Phys Soc London Sect B64:747
21. Petch NJ (1953) J Iron Steel Inst 174:25
22. Macionczyk F, Bruckner W (1999) J Appl Phys 86:4922
23. Mathur A, Erlebacher J (2007) Appl Phys Lett 90:061910
24. Qiao L, Zheng X (2008) Appl Phys Lett 92:231908
25. UDEL Polysulfone Design Guide (2002) Solvay advanced polymers. Alpharetta, GA
26. Loría-Bastarrachea MI, Vázquez-Torres H, de Aguilar-Vega MJ (2002) J Appl Polym Sci 86:2515
27. Zhang JM, Zhang Y, Xu KW, Ji V (2007) J Phys Chem Solids 68:503
28. Várguez P, Avilés F, Oliva AI (2008) Surf Coat Technol 202:1556
29. Chiu SL, Leu J, Ho PS (1994) J Appl Phys 76:5136
30. Gere JM, Timoshenko SP (1984) Mechanics of materials. Wadsworth Inc., Monterey
31. Mitchell BS (2004) An introduction to materials engineering and science. Wiley-Interscience, Hoboken
32. Gadelhak M (2002) The MEMS handbook. CRC Press, New York
33. Stalder A, During U (1996) Appl Phys Lett 68:637
34. Cao Y, Allameh S, Nankivil D, Sethiaraj S, Otiti T, Soboyejo W (2006) Mater Sci Eng A 427:232
35. Gu QF, Krauss G, Steurer W, Gramm F, Cervellino A (2008) Phys Rev Lett 100:045502
36. Yang SH, Wei ZX (2008) Phys B 403:559
37. Diao J, Gall K, Dunn M-L (2004) Nano Lett 4:1863–1867
38. Venkatraman R, Bravman JC (1992) J Mater Res 7:2040
39. Keller RM, Baker SP, Artz E (1998) J Mater Res 13:1307
40. Nemat-Nasser S, Maximenko A, Olevsky E (2006) J Mech Phys Solids 54:2474